

Contents lists available at ScienceDirect

## Journal of Alloys and Compounds

journal homepage: http://www.elsevier.com/locate/jalcom



## Precipitation strengthening in aluminum-zirconium-vanadium alloys



Yangyang Fan, Makhlouf M. Makhlouf\*

Department of Mechanical Engineering, Worcester Polytechnic Institute, Worcester, MA, 01609, USA

#### ARTICLE INFO

Article history: Received 10 April 2017 Received in revised form 11 July 2017 Accepted 13 July 2017 Available online 17 July 2017

Keywords: Precipitation strengthening Shell-and-core structure Anti-phase boundary energy

#### ABSTRACT

Atom probe tomography (APT) and high resolution transmission electron microscopy (HRTEM) were used to study the co-precipitation and coarsening mechanisms of  $Al_3(Zr_{1-x_i}V_x)$  precipitates formed in Al-Zr-V alloys. The strengthening mechanism that is operative in properly aged Al-Zr-V alloys are determined, and the antiphase boundary (APB) energy between the  $\alpha$ -Al matrix and the  $Al_3(Zr_{1-x_i}V_x)$  precipitates is indirectly determined.

© 2017 Elsevier B.V. All rights reserved.

#### 1. Introduction

Extensive work has been performed on alloying aluminum with transition metals (TM) particularly scandium [1,2] and zirconium [3–5], and combinations of scandium and zirconium [6–14]; because, upon proper heat-treatment of the alloy, these elements tend to form precipitates that have the chemical composition Al<sub>3</sub>TM and the L1<sub>2</sub> crystal structure. These precipitates tend to be thermally stable, and when they are present in large volume fractions, they significantly increase the high temperature yield strength of aluminum alloys [8,11]. For these reasons, Al-TM alloys are often thought of as excellent candidates for high temperature applications. However, the strength of Al-Sc alloys deteriorates when they are used at temperatures above 300 °C [15]. This is mainly due to the high diffusivity of scandium in aluminum at these temperatures (D<sub>Sc</sub> = 1.98  $\times$  10<sup>-17</sup> m²/s at 400 °C [16]) and the low thermal stability of the Al<sub>3</sub>Sc phase at temperature above 300 °C.

The L1<sub>2</sub>-Al<sub>3</sub>Zr phase is more thermally stable than the L1<sub>2</sub>-Al<sub>3</sub>Sc phase at elevated temperatures. And many studies have attempted to further stabilize it by alloying it with Ti or V to form coprecipitates of the general formula  $Al_3(Zr_{1-x},TM_x)$  [17–20]. For example, Fine and Chen [19,20] reported that by adding V to Al-Zr alloys, the coarsening rate of the precipitates that form is significantly lowered. Fine [21] attributed this phenomenon to a lowering of the lattice parameter mismatch between the precipitate particles and the aluminum matrix upon adding V. However, details of the

mechanism of formation of the  $Al_3(Zr_{1-x}V_x)$  co-precipitate remains unclear.

In this study, we employed atom probe tomography (APT) and HRTEM to study the co-precipitation and coarsening mechanisms of  $Al_3(Zr_{1-x},V_\chi)$  precipitates formed in Al-Zr alloys with various V contents. Moreover, we define the strengthening mechanism that is operative in these Al-Zr-V alloys, and we estimate — albeit indirectly — the Al-Al<sub>3</sub>Zr and Al- Al<sub>3</sub>(Zr<sub>1-x</sub>,V<sub>\chi</sub>) antiphase boundary (APB) energies.

#### 2. Materials and procedures

#### 2.1. Alloy preparation and heat-treatment

The Al-Zr-V alloys shown in Table 1 were constituted from pure aluminum ingots (99.99% purity), and Al-65wt%V and Al-15wt%Zr master alloys. The alloys were melted in air in an induction furnace in clean silicon carbide crucibles coated with boron nitride. The melts were degassed with high purity argon gas by means of a rotating impeller degasser for 30 min, and they were poured at approximately 800 °C in a water-cooled copper mold. This mold produces ASTM standard sub-size tensile test specimens that solidify with a uniform cooling rate of about 120 °C/s into a super-saturated solid solution. The as-cast specimens were isothermally aged in an electric furnace at 400 °C and 450 °C for various times ranging from 1 to 150 h, and then cooled from the aging temperature to room temperature in air.

<sup>\*</sup> Corresponding author. E-mail address: mmm@wpi.edu (M.M. Makhlouf).

**Table 1**Nominal chemical composition of the alloys.

Alloy	Zirconium		Vanadium		Aluminum
	wt. %	at. %	wt. %	at. %	
A1	0.40	0.18	0.00	0.00	Balance
A2	0.80	0.24	0.40	0.21	Balance
A3	0.40	0.12	0.40	0.21	Balance
A4	0.10	0.03	0.40	0.21	Balance

#### 2.2. Microstructure analysis

Samples from the alloys of Table 1 were prepared for scanning electron microscopy (SEM) by polishing according to standard metallographic methods and etching with Kelly's reagent. A JOEL-7000F scanning electron microscope operating at 15 kV was used for the analyses. Samples from the alloys of Table 1 were also prepared for transmission electron microscopy (TEM) by thinning foils cut from the alloys to perforation by means of a twinjet electro-polisher (Fischione Instruments, model 120) operating at 12 V, and utilizing a solution of 10 vol% perchloric acid in methanol maintained at  $-20~^{\circ}$ C. A JOEL-2010F transmission electron microscope (TEM) was used to measure the size of the precipitate particles. A minimum of 200 particles were analyzed from each sample in order to obtain the mean precipitate size. An aberration corrected MC Zeiss 200-80 TEM operating at 200 kV was used to perform high-resolution microstructure analysis.

#### 2.3. Mechanical properties

The tensile properties of the alloys were measured by means of a Universal Testing machine (Instron model 5500R) at an extension rate of 0.05 in/min, and a 1-inch gage length extensometer (MTS model 634.25E-24) was used to measure extension. At least 5 specimens from each alloy were used and the results were averaged and standard deviations were calculated. Fracture of all specimens occurred within the gage length, and specimens with excessive porosity and/or oxides that would affect the results were excluded from the average.

#### 2.4. Atom probe tomography

Specimens cut from Alloy A2 of Table 1 were aged at 400 °C for 32 h and then they were examined by Atom Probe Tomography (APT). The APT specimens were prepared by the standard lift-out technique in a dual-beam focused ion beam/scanning electron microscopy workstation (FIB/SEM) (Helios NanoLab 600TM, FEI Company, USA). Two lift-outs including several samples were extracted from the middle of two Al dendrites. After thinning of the samples, a low energy milling at 2 kV was performed in order to minimize Ga induced damage. APT was performed in a LEAPTM 3000X HR (CAMECA) in voltage mode at 20% pulse fraction and a repetition rate of 200 kHz. Specimen temperature of about 60 K, pressure lower than  $1 \times 10^{-10}$  Torr (1.33  $\times$  10<sup>-8</sup> Pa) and evaporation rate of 5 atoms per 1000 pulses were used for all measurements. Datasets were reconstructed and analyzed with the IVASTM 3.6.6 software (CAMECA). Overall compositions were measured after background noise subtraction, and all measurements were averaged by weighting the averages based on the total number of atoms of each measurement. The randomness of the atomic distribution in the APT specimens was evaluated by a frequency distribution analysis where the actual distribution of atoms is compared to a completely random dataset described by a binomial probability distribution. The departure from randomness was quantified by a chi-square analysis which allows a significance test. A significance value p < 0.01 was chosen to reject the null hypothesis and indicate that there is significant deviation from randomness in the arrangements of atoms through the dataset. Localized chemical profile of the precipitates was performed using zirconium isoconcentration surfaces and proximity histograms.

#### 3. Results

#### 3.1. As-cast microstructure

Fig. 1 shows a typical SEM photomicrograph taken from an ascast A3 alloy sample. The sample was etched so its dendrite structure is revealed. Careful examination of this and many similar photomicrographs taken from the alloys in Table 1 show no primary phase precipitates, which suggests that the fast cooling rate that was used in making these samples suppressed precipitation, and allowed formation of a supersaturated  $\alpha$ -Al solid solution, even though the zirconium and/or vanadium content of the alloys may exceed their solubility limit in aluminum.

#### 3.2. Room-temperature mechanical properties

Fig. 2 shows the variation in the measured yield strength of alloys A2, A3, and A4 with aging time at 400 °C and 450 °C. It is clear that at both aging temperatures the yield strength of the three alloys peaks after about 32 h, and alloy A2 has the highest yield strength. Holding the alloys at these temperatures for longer times does not significantly change their yield strength.

#### 3.3. Aged microstructure

Fig. 3 shows typical HRTEM images of samples from alloys A2, A3, and A4 that were aged at 400 °C for 32 h. The strain and Z contrast of the  $Al_3(Zr_{1-x},V_x)$  precipitate particles can be clearly distinguished in these images. Alloy A2 has the highest volume fraction of  $L1_2$ -Al $_3(Zr_{1-x},V_x)$  particles and alloy A4 has the lowest, which is consistent with the measured yield strength of these alloys (see Fig. 2). The strain and Z contrast of the precipitate particles can be clearly distinguished in these images. The precipitate particles in all three alloys are 4–6 nm in diameter, and the particles are fully coherent with the aluminum matrix. As Fig. 3(d) shows, the samples were tilted to the [100] zone axis and the superalattice diffraction pattern contributed by  $L1_2$  phase can be clearly seen. Therefore, it is reasonable to conclude that these particles are  $Al_3(Zr,V)$  precipitates with  $L1_2$  crystal structure.

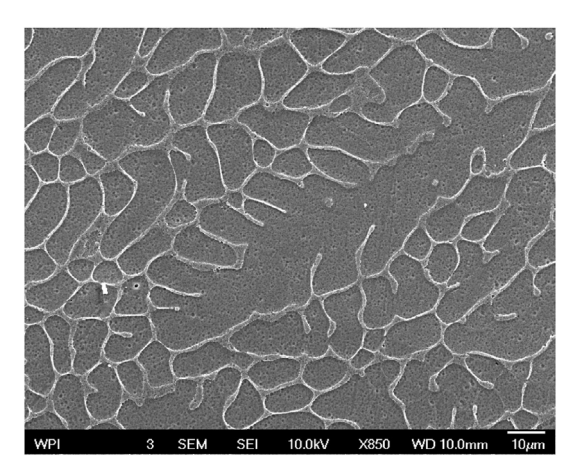


Fig. 1. SEM photomicrograph of as-cast alloy A3 of Table 1.

### Download English Version:

# https://daneshyari.com/en/article/5458334

Download Persian Version:

https://daneshyari.com/article/5458334

<u>Daneshyari.com</u>